8-2012

Origin Of Fluorescence In 11-cis Locked Bovine Rhodopsin

Elena N. Laricheva

Samer Gozem

Silvia Rinaldi

Federico Melaccio

Alessio Valentini

See next page for additional authors

JCTC Journal of Chemical Theory and Computation
Letter
pubs.acs.org/JCTC

Origin of Fluorescence in 11-*cis* Locked Bovine Rhodopsin

Elena N. Laricheva,[†] Samer Gozem,[†] Silvia Rinaldi,[‡] Federico Melaccio,[‡] Alessio Valentini,[‡] and Massimo Olivucci[†,‡,*]

[†]Department of Chemistry, Center for Photochemical Sciences, Bowling Green State University, Bowling Green, Ohio 43403, United States

[‡]Dipartimento di Chimica, Università di Siena, via De Gasperi 2, I-53100 Siena, Italy

Supporting Information

ABSTRACT: The excited state lifetime of bovine rhodopsin (Rh) increases from ca. 100 fs to 85 ps when the C11=C12 bond of its chromophore is locked by a cyclopentene moiety (Rh5). To explain such an increase, we employed *ab initio* multiconfigurational quantum chemistry to construct computer models of Rh and Rh5 and to investigate the shape of their excited state potential energy surfaces in a comparative way. Our results show that the observed Rh5 fluorescence (λ_{max}^{f} = 620 nm) is due to a previously unreported locally excited intermediate whose lifetime is controlled by a small energy barrier. The analysis of the properties and decay path of such an intermediate provides useful information for engineering rhodopsin variants with augmented fluorescence efficiencies.

In the rapidly advancing field of *in vivo* imaging, the development of fluorescent proteins (FPs) is highly desirable,[1,2] especially for optogenetics needs[3−5] where novel, genetically encodable fluorescent probes are required. Currently, the majority of FPs is based on engineered variants of the green fluorescent protein (GFP) from the jellyfish *Aequorea victoria* and its homologues from other marine organisms.[6,7] However, in order to further expand the existing FPs toolbox, it would be advantageous to have light-emitting proteins with no homology to GFP, especially because the latter has a few drawbacks such as insufficient speed of chromophore maturation controlled by the presence of oxygen in the system, ease of photobleaching, and a low signal-to-noise ratio.[8,9] Here, we report the results of a computational study indicating that members of the rhodopsin family may be engineered to yield alternative sources of FPs, despite the ultrafast photoisomerization reaction characterizing these systems.

Recently, Kralj and co-workers have discovered two microbial rhodopsin-based voltage-sensitive fluorescent proteins: proteorhodopsin optical proton sensor (PROPS)[10] and archaerhodopsin 3 (Arch).[11] The authors have suggested further exploring the family of microbial rhodopsins for the ability to fluoresce: novel rhodopsin-based FPs would become a great addition to the category of optogenetics tools called reporters. Accordingly, a systematic mutagenesis and directed evolution of PROPS and Arch, as well as the high-throughput screening of microbial genomes for their homologues, represents one possible way to generate new reporters. Another strategy is to turn a known nonfluorescent rhodopsin into a fluorescent one by finding a way to increase the excited state lifetime of its chromophore so that fluorescence becomes competitive with ultrafast photoisomerization and nonradiative deactivation. To design this type of system, the use of quantum chemical models is crucial. One first needs to unveil the structural basis for the optical properties of nonfluorescent rhodopsin by computing the electronic structure of the opsin-embedded chromophore, understand its interactions with the apoprotein in both ground and excited states, and gain insights into the mechanism of the photoisomerization reaction. In this context, the well-studied[12−16] bovine rhodopsin (Rh) represents a good "laboratory" system.

Numerous experimental[13,17,18] and theoretical[14−16,19,20] studies of Rh already confirmed that the ultrafast *cis* to *trans* photoisomerization of the 11-*cis* retinal protonated Schiff base (PSB11) is driven by a barrierless excited state (S_1) path connecting the Franck−Condon point (FC) to the conical intersection (CI; path 1, Figure 1A). This results in an extremely short S_1 lifetime (τ_{fl} ca. 100 fs[17]) and emission with a negligibly small quantum yield ($\Phi_f = 1.2 \times 10^{-5}$).[21] However, in principle, one can significantly increase τ_{fl} by imposing the S_1 barrier (TS) on the way from the fluorescent state (FS) to the CI (path 2, Figure 1A).

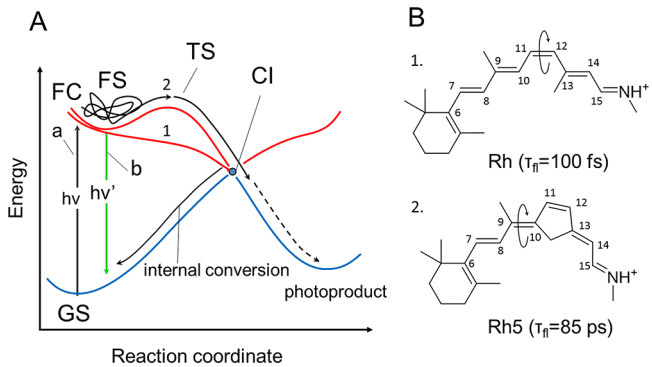

Figure 1. (A) Schematic representation of the barrierless (1) and barrier-controlled (2) S_1 path (a, absorption; b, emission). (B) Chemical structures of the retinal in Rh and Rh5. The curly arrows indicate the corresponding reactive double bonds.

Received: March 27, 2012
Published: July 18, 2012

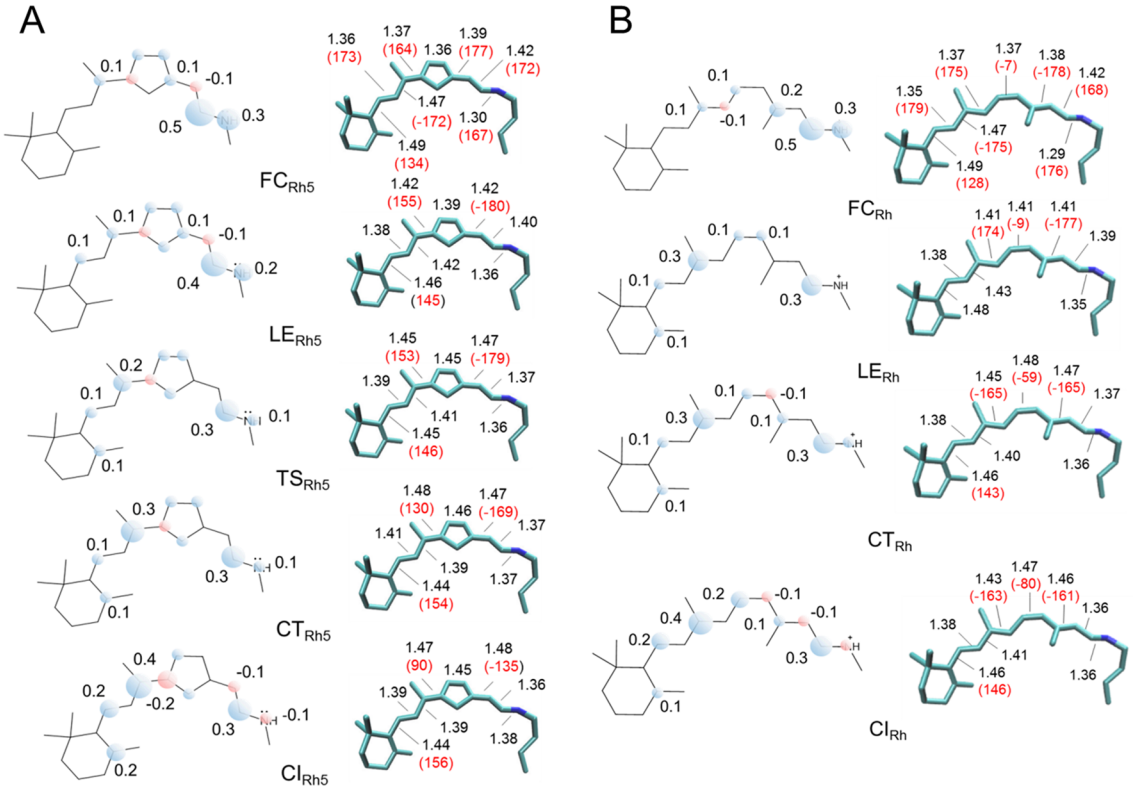

Figure 2. Charge distribution and relevant geometrical parameters (bond lengths in Ångstroms, black, and dihedral angles in degrees, red) of the stationary points along the S_1 path of Rh5 (A) and Rh (B).

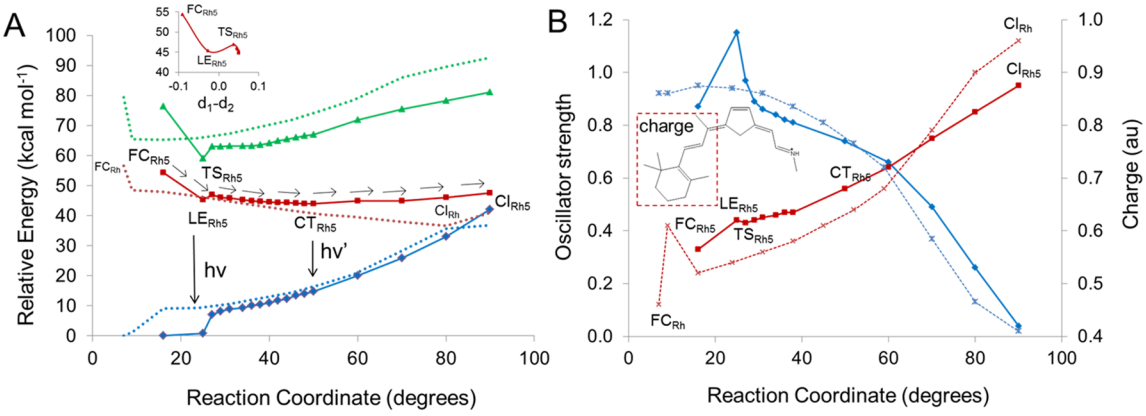

Figure 3. (A) S_2 (green), S_1 (red), and S_0 (blue) energies along a three-root state average (equal weights) CASPT2//CASSCF/6-31G*/AMBER S_1 relaxed scan of Rh5 (solid lines) from the FC_{Rh5} to the CI_{Rh5} along the reaction coordinate corresponding to the C8−C9−C10−C11 dihedral angle and describing the torsion of the C9═C10 bond. Since the LE_{Rh5} and TS_{Rh5} have very close C8−C9−C10−C11 values, the *same* energies were reported along the d_1−d_2 stretching coordinate (see insert at the top) that was found to undergo the major geometrical change in the FC_{Rh5} to TS_{Rh5} region where the double bonds expand while the single bonds contract. A detailed description of the reaction coordinate defining the S_1 path is given in section S3 of the Supporting Information. For comparison, the dotted lines represent the S_1 relaxed scan (driven by the C10−C11−C12−C13 dihedral angle) in Rh where the torsional deformation involves the C11═C12 bond. The d_1−d_2 reaction coordinate (in Ångstroms) shown in the insert represents the difference between the average sum of all the formal single bonds (d_1) and all formal double bonds (d_2). (B) Change in oscillator strength (blue) and amount of the positive charge (red) on the framed fragment (i.e., the one starting at ═C9−C8═ and containing the *β*-ionone ring) along the S_1 path in Rh5 (solid lines) and Rh (dotted lines).

One extreme way to do so is to restrain the isomerization of the C11═C12 bond by locking it with a cyclic moiety (Figure 1B). Several experimental studies were performed in this direction. The biggest τ_{fl} increase (85 ps) along with a fluorescence signal (λ_{max}^{f} = 620 nm) and no photoproduct formation was observed by Kandori and co-workers[17,22] for the Rh analogue with an 11-*cis* double bond incorporated in a cyclopentene ring (Rh5). The results of this experiment were used to confirm that *cis*/*trans* isomerization is a primary event in vision. However there were no attempts to look at such a result as a demonstration that rhodopsins can be turned into fluorescent proteins. Below, we construct hybrid quantum mechanics/molecular mechanics (QM/MM)[23,24] models of both Rh and Rh5 to study the origin of the observed fluorescence increase in a comparative way.

dx.doi.org/10.1021/ct3002514 | J. Chem. Theory Comput. 2012, 8, 2559−2563

The CASPT2//CASSCF/6-31G*/AMBER QM/MM protocol used in this work is based on the electrostatic embedding[24−26] and hydrogen link atom (LA) schemes.[27] Previously, it has proved its validity to provide structures and excitation energies consistent with experimental observables.[19,20,28] The basic methodology is described in ref 29. Additional details, specific for this study, are given in the Supporting Information (see section S1). The models of Rh and Rh5 are based on the 2.2 Å resolution 1U19[30] crystal structure. The locked one is generated by incorporating the C11═C12 bond in a cyclopentene ring. With the exception of the Glu113 counterion, the Rh cavity is set to neutral. The chromophore, the position/orientation of two TIP3P water molecules, the Lys296 side chain, and the side chains of all cavity residues located within 4 Å from the chromophore are relaxed during the geometry optimization. At the equilibrium geometries, computed at the CASSCF/6-31G*/AMBER level, three-root state average CASPT2 calculations are performed to evaluate the absorption (λ_{max}^{a}) and fluorescence (λ_{max}^{f}) maxima and the oscillator strengths (f) of the S_0-S_1 and S_0-S_2 transitions.

The quality of the above QM/MM protocol was assessed by modeling the λ_{max}^{a} values of Rh and Rh5. Our results show that the ground state (S_0) equilibrium geometries of Rh and Rh5 (FC_{Rh} and FC_{Rh5}) yield close computed λ_{max}^{a} values (505 and 526 nm, respectively), in line with very close observed values (498 nm[22,31] and 495 nm,[22] respectively) and consistently with a 3.0 kcal·mol^{-1} excitation energy error (see the Supporting Information, Table S1 for details). As the close λ_{max}^{a} values of Rh and Rh5 suggest, the FC_{Rh5} and FC_{Rh} geometries should be similar.

Our calculations confirm this: both chromophores have twisted structures with a negative (counter-clockwise) helicity and similar geometrical parameters (see Figure 2A and B for Rh5 and Rh, respectively). However, due to the presence of the cyclopentene ring, the Rh5 backbone is more bent. In fact, the C6−N distances in Rh5 and Rh are 10.2 Å and 11.3 Å, respectively.

As a result of the S_1 geometry optimization in Rh5, the existence of two energy minima, LE_{Rh5} and CT_{Rh5}, separated by a small energy barrier (ca. 2.0 kcal·mol^{-1} according to a relaxed scan), was established (Figures 2A and 3A). Figure 2A shows that these structures differ by the charge distribution, amount of bond length alternation (BLA), and degree of torsion around the C9═C10 bond. Indeed, along the S_1 path of Rh5, the C8−C9−C10−C11 dihedral is coupled with the bond stretching reflected by a change in BLA and quantified by the d_1-d_2 value. In particular, as documented in Figure 2, the S_1 relaxation is initially dominated by bond stretching, while beyond the transition state the change in the C8−C9−C10−C11 dihedral dominates over the stretching, which remains substantially constant. The CT_{Rh5} has a charge-transfer character and features a strong BLA pattern similar to a loose nonfluorescent S_1 intermediate previously reported by Andruniow et al.[19] for Rh. The LE_{Rh5}, located just 1.0 kcal·mol^{-1} above CT_{Rh5}, is characterized by a BLA pattern closer to the S_0 state and featuring equally stretched bonds in the middle part of the chromophore backbone. We refer to LE_{Rh5} as a locally excited state. To the best of our knowledge, this is a novel (previously not reported) rhodopsin intermediate located closer to the FC point in terms of geometry and electronic structure. On the other hand, in the literature, the simultaneous presence of an "LE state" and a "CT state" is widely used to describe the phenomenon of dual fluorescence in many fluorophores, with the LE state being responsible for emission at short wavelengths before the charge separation and formation of the CT state (often twisted) occurs.[32−34]

The experimentally observed fluorescence in Rh5 (λ_{max}^{f} = 620 nm) originates from the LE_{Rh5} state. Indeed (see the Supporting Information, Table S1 for details), the λ_{max}^{f} computed for LE_{Rh5} (644 nm) correlates well with the experimental observable (620 nm[22]), while for CT_{Rh5} the value is too red-shifted (979 nm). The oscillator strength computed for LE_{Rh5} (f = 1.0) is also higher than for the CT_{Rh5} (f = 0.7). Recently, Valsson and Filippi[35] have investigated the structural relaxation in the S_1 state of different gas-phase models of the retinal chromophores using the CASSCF, CASPT2, quantum Monte Carlo (QMC), and coupled cluster (CC) methods. In contrast with CASSCF, the CASPT2, QMC, and CC results reveal the existence of an S_1 minimum similar to the LE_{Rh5} (located at the CASSCF/AMBER level). This suggests that such an intermediate is stabilized by the modeled protein environment, and that, in such an environment, it requires less dynamic electron correlation to exist. Similar results have been recently reported by Muños-Losa et al.,[36] who simulated a five double-bond retinal chromophore model in methanol solution. For this model, the authors have been able to locate two different S_1 energy minima at the CASSCF/MM level: one displaying similar bond lengths and a small BLA value and another one ionic with a pronounced BLA pattern. These findings have been used to reinterpret the fluorescence spectrum of the all-*trans* retinal chromophore in methanol reported by Zgrablic et al.[37] in terms of dual fluorescence with the high-frequency part of the fluorescence band assigned to a "covalent" S_1 minimum and the low-frequency one to a charge-transfer S_1 minimum. This situation is similar to the one reported here for Rh5.

According to our results, LE (LE_{Rh}) and CT (CT_{Rh}) regions also exist in Rh (Figure 2B), but they are unstable. In contrast to Rh5, the CT_{Rh} region is located 9.0 kcal mol^{-1} below the LE_{Rh} region with no barrier separating the two structures (Figures 3A and S2). As we will discuss below, these differences can be explained on the basis of the resonance stabilization of the translocated positive charge along the chromophore backbone.

To improve our understanding of the mechanisms driving the S_1 decay in Rh5 and Rh, we also located the structures of the low-lying S_1/S_0 CI for each case (CI_{Rh5} and CI_{Rh}, respectively). The CI_{Rh} was extensively studied in the past, and its computed structure (Figure 2B), featuring an 80° twist of the C11═C12 bond, correlates well with the previous studies.[19,20,28,38] In contrast, in Rh5 the isomerization around the C11═C12 bond is restricted due to the presence of a cyclopentene ring, and therefore, CI_{Rh5} features a fully twisted neighboring C9═C10 bond (Figure 2A). This is consistent with the notion that the reported S_1 isomerization coordinate of Rh has a bicycle-pedal[16] nature where the reactive C11═C12 twisting is accompanied by a partial twisting of the adjacent C9═C10 bond. Thus, it is apparent that if one blocks the rotation of the C11═C12 bond, the C9═C10 undergoes the photoisomerization more likely than the C13═C14. Indeed, Jang et al.[39] observed the isomerization of the C9═C10 rather than the C13═C14 bond in a rhodopsin analogue with the retinal chromophore locked by a cyclohexene ring.

As Figures 3A and S2 show, in Rh the evolution of the S_1 population from the FC_{Rh} to the CI_{Rh} is driven by a

dx.doi.org/10.1021/ct3002514 | J. Chem. Theory Comput. 2012, 8, 2559−2563

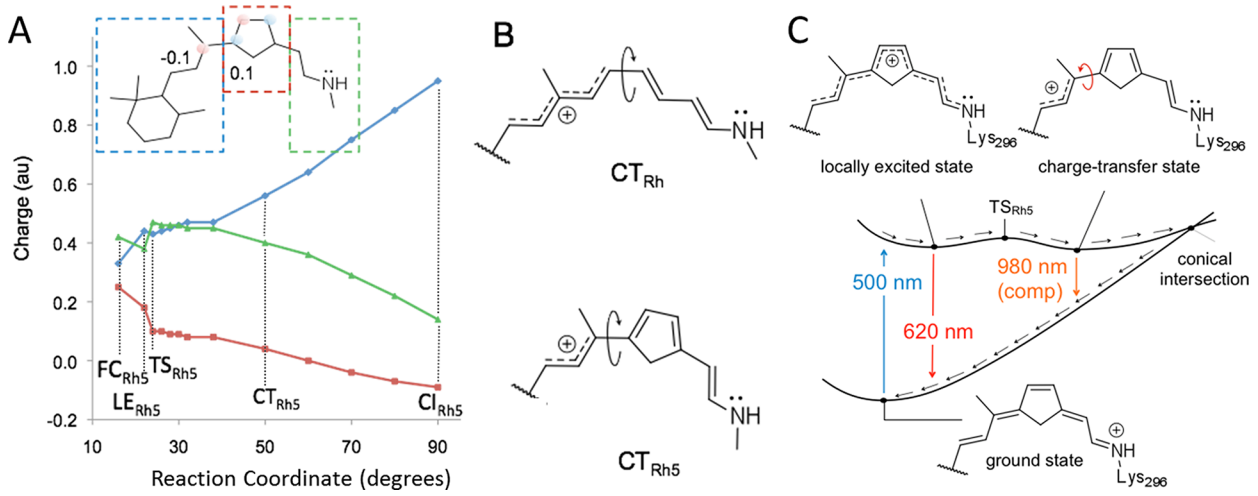

Figure 4. (A) Differential (LE_{Rh5}−CT_{Rh5}) charge distribution (top) and changes in the amounts of positive charge on the C1−C9 (blue), C10−C12 (red), and C13−N (green) fragments along the S_1 path of Rh5. (B) Representation of the charge delocalization on the pentadienyl fragment in Rh and allyl—in Rh5. (C) Schematic representation of the fluorescence generation in Rh5. The formulas indicate the electronic structures characterizing the ground state and two different fluorescent states located on the spectroscopic state of the protein.

substantially barrierless reaction path consistent with previous results.[19,20] Thus, LE_{Rh} corresponds to a flat region from where the chromophore quickly relaxes to CI_{Rh} passing through a CT_{Rh} structure located along a steeper S_1 path region. This is consistent with the subpicosecond excited state lifetime (ca.100 fs) seen for Rh. In contrast, the S_1 energy profile of Rh5 is shallow (Figure 3A). While in Rh the CT_{Rh} is located 9 kcal mol^{-1} below the LE_{Rh}, in Rh5 the CT_{Rh5} is only 1.1 kcal mol^{-1} more stable than the LE_{Rh5}. The transition state (TS_{Rh5}) separating the LE_{Rh5} and CT_{Rh5} regions is responsible for the substantial increase in the fluorescent lifetime observed experimentally (85 ps), which is assigned to the LE_{Rh5} structure. Note that, in spite of the reported ca. 3.0 kcal·mol^{-1} error in the computed excitation energies, the similarity in the geometry and electronic structure of LE_{Rh5} and TS_{Rh5} should lead to error cancellation when computing their energy difference relative to a common reference (e.g., the FC_{Rh5}). Therefore, we believe that a ca. 2.0 kcal·mol^{-1} computed energy barrier responsible for the increase of fluorescence represents a meaningful estimate (assuming that the error cancels out at least partially).

As reported in Figure 3B, the charge-transfer character of the S_1 wave function, revealed by the 0.4−0.5 au increase in the charge residing on the β-ionone fragment of the chromophore, is maintained along the S_1 path in both Rh5 and Rh. The general trend in the change of oscillator strength (f) along the S_1 path in these two models is also similar: starting from the FC point the f increases, reaches a maximum, and then constantly decreases when approaching the intersection region. However, in Rh5 the initial increase of the f is larger with a maximum of the curve corresponding to the fluorescent LE_{Rh5} structure.

As the shape of the barrier-controlled S_1 path in Rh5 suggests, a preferential stabilization of LE_{Rh5} with respect to CT_{Rh5} should yield a further increase in $\tau_{fl.}$ The analysis of the differential charge distribution (Figure 4A) indicates that a promising strategy for LE_{Rh5} stabilization could be to increase the negative electrostatic potential projected by the amino acid residues on the middle part of the chromophore. In fact, a bigger fraction of the positive charge is localized on the ═C10−C11═C12− fragment in LE_{Rh5} compared to CT_{Rh5}.

Our calculations suggest that the S_1 barrier corresponding to the TS_{Rh5} is mainly due to electronic effects and can be explained by resonance stabilization and the Hammond postulate.[40] In fact, upon twisting of the C11═C12 bond in Rh, the positive charge, initially located on the −N═C15 moiety, is gradually translocated along the chromophore backbone toward the β-ionone ring. This process ultimately leads to a full positive charge delocalized on the −C7═C8−C9═C10−C11═ pentadienyl fragment (Figure 4B, top). In contrast, in Rh5, where the C9═C10 bond twists, the charge is delocalized on the shorter −C7═C8−C9═ allyl fragment (Figure 4B, bottom). This produces a less stable resonance hybrid of the (product) charge-transfer state in the locked model relative to the unlocked one. The Hammond postulate explains the flattening of the S_1 energy profile and the presence of a small energy barrier separating the LE_{Rh5} and CT_{Rh5} structures (see section S4 in the Supporting Information for details) as confirmed by our calculations. To corroborate the intramolecular origin of the barrier, we recomputed the energy profile along the S_1 path of Rh5 in the absence of the protein (see the Supporting Information, Figure S4) and demonstrated that the flat S_1 energy surface of the locked system is mainly a consequence of its reaction coordinate (i.e., of the structural changes imposed by the protein cavity). This indicates that one could increase the LE_{Rh5} lifetime by increasing the Rh5 barrier for the S_1 isomerization of the C9═C10 bond via steric and electrostatic interactions. In particular, the proximity of the T118 and Y268 residues to the chromophore C9-methyl group suggests that they could play a role in increasing the barrier.

In conclusion, our QM/MM models support the mechanism displayed in Figure 4C. The observed Rh5 fluorescence (620 nm) is assigned to a locally excited intermediate featuring an untwisted backbone with a BLA pattern still not completely inverted with respect to S_0. The same calculations predict the existence of a second red-shifted fluorescent intermediate with a full charge-transfer character at ca. 980 nm, which, to the best of our knowledge, has not been spectroscopically investigated. These results provide the basis for engineering rhodopsin-based fluorescent proteins with a chemical modification of the chromophore and, possibly, suitable mutations. In perspective, we plan to construct and study a series of the QM/MM mutant

dx.doi.org/10.1021/ct3002514 | J. Chem. Theory Comput. 2012, 8, 2559−2563

models with amino acid substitutions that stabilize the positive charge in the middle part of the retinal and increase the steric hindrance for the rotation around the C9=C10 bond. The combination of these effects could be advantageous. If these tests are positive, Rh5 may be a promising system for engineering novel fluorescent pigments with no homology to GFP.

■ ASSOCIATED CONTENT

Supporting Information

Details of the QM/MM protocol. Computed S_1 paths of Rh5 and Rh. Explanation on how Hammond postulate applies to Rh5 vs Rh case. Table (Table S1) of the relative energies, computed and experimental $\lambda_{max}{}^{a}$ and $\lambda_{max}{}^{f}$, and f values. Figure S1–S5. Table of the Cartesian coordinates of the stationary points of Rh and Rh5. This material is available free of charge via the Internet at http://pubs.acs.org.

■ AUTHOR INFORMATION

Corresponding Author

*E-mail: molivuc@bgsu.edu.

Notes

The authors declare no competing financial interest.

■ ACKNOWLEDGMENTS

This work was supported by the Bowling Green State University. M.O. is grateful to the Center for Photochemical Sciences of Bowling Green State University for start-up funds. We thank the Ohio Supercomputer Center for granted computer time.

■ REFERENCES

(1) Lippincott-Schwartz, J.; Patterson, G. H. *Science* **2003**, *300*, 87–91.
(2) Mehta, S.; Zhang, J. *Annu. Rev. Biochem.* **2011**, *80*, 375–401.
(3) Knöpfel, T.; Lin, M. Z.; Levskaya, A.; Tian, L.; Lin, J. Y.; Boyden, E. S. *J. Neurosci.* **2010**, *30*, 14998–15004.
(4) Moglich, A.; Moffat, K. *Photochem. Photobiol. Sci.* **2010**, *9*, 1286–1300.
(5) Baker, M. *Nat. Methods* **2011**, *8*, 19–22.
(6) Chudakov, D. M.; Lukyanov, S.; Lukyanov, K. A. *Trends Biotechnol.* **2005**, *23*, 605–613.
(7) Day, R. N.; Schaufele, F. *J. Biomed. Opt.* **2008**, *13*, 031202.
(8) Zhang, J.; Campbell, R. E.; Ting, A. Y.; Tsien, R. Y. *Nat. Rev. Mol. Cell Biol.* **2002**, *3*, 906–918.
(9) Fernandez-Suarez, M.; Ting, A. Y. *Nat. Rev. Mol. Cell Biol.* **2008**, *9*, 929–943.
(10) Kralj, J. M.; Hochbaum, D. R.; Douglass, A. D.; Cohen, A. E. *Science* **2011**, *333*, 345–348.
(11) Kralj, J. M.; Douglass, A. D.; Hochbaum, D. R.; Maclaurin, D.; Cohen, A. E. *Nat. Methods* **2012**, *9*, 90–95.
(12) Kandori, H.; Shichida, Y.; Yoshizawa, T. *Biochemistry (Moscow)* **2001**, *66*, 1197–1209.
(13) Polli, D.; Altoe, P.; Weingart, O.; Spillane, K. M.; Manzoni, C.; Brida, D.; Tomasello, G.; Orlandi, G.; Kukura, P.; Mathies, R. A.; Garavelli, M.; Cerullo, G. *Nature* **2010**, *467*, 440–443.
(14) Warshel, A.; Barboy, N. *J. Am. Chem. Soc.* **1982**, *104*, 1469–1476.
(15) Warshel, A.; Chu, Z. T.; Hwang, J. *Chem. Phys.* **1991**, *158*, 303–314.
(16) Warshel, A. *Nature* **1976**, *260*, 679–683.
(17) Kandori, H.; Furutani, Y.; Nishimura, S.; Shichida, Y.; Chosrowjan, H.; Shibata, Y.; Mataga, N. *Chem. Phys. Lett.* **2001**, *334*, 271–276.
(18) Schoenlein, R.; Peteanu, L.; Mathies, R.; Shank, C. *Science* **1991**, *254*, 412–415.
(19) Andruniów, T.; Ferré, N.; Olivucci, M. *Proc. Natl. Acad. Sci. U. S. A.* **2004**, *101*, 17908–17913.
(20) Frutos, L. M.; Andruniów, T.; Santoro, F.; Ferré, N.; Olivucci, M. *Proc. Natl. Acad. Sci. U. S. A.* **2007**, *104*, 7764–7769.
(21) Doukas, A. G.; Junnarkar, M. R.; Alfano, R. R.; Callender, R. H.; Kakitani, T.; Honig, B. *Proc. Natl. Acad. Sci. U. S. A.* **1984**, *81*, 4790–4794.
(22) Kandori, H.; Matuoka, S.; Shichida, Y.; Yoshizawa, T.; Ito, M.; Tsukida, K.; Balogh-Nair, V.; Nakanishi, K. *Biochemistry* **1989**, *28*, 6460–6467.
(23) Warshel, A.; Levitt, M. *J. Mol. Biol.* **1976**, *103*, 227–249.
(24) Senn, H. M.; Thiel, W. *Angew. Chem., Int. Ed.* **2009**, *48*, 1198–1229.
(25) Lin, H.; Truhlar, D. *Theor. Chem. Acc.* **2007**, *117*, 185–199.
(26) Ferré, N.; Ángyán, J. G. *Chem. Phys. Lett.* **2002**, *356*, 331–339.
(27) Singh, U. C.; Kollman, P. A. *J. Comput. Chem.* **1986**, *7*, 718–730.
(28) Schapiro, I.; Ryazantsev, M. N.; Frutos, L. M.; Ferré, N.; Lindh, R.; Olivucci, M. *J. Am. Chem. Soc.* **2011**, *133*, 3354–3364.
(29) Ferré, N.; Olivucci, M. *THEOCHEM* **2003**, *632*, 71–82.
(30) Okada, T.; Sugihara, M.; Bondar, A.; Elstner, M.; Entel, P.; Buss, V. *J. Mol. Biol.* **2004**, *342*, 571–583.
(31) Hurley, J. B.; Ebrey, T. G.; Honig, B.; Ottolenghi, M. *Nature* **1977**, *270*, 540–542.
(32) Cogan, S.; Zilberg, S.; Haas, Y. *J. Am. Chem. Soc.* **2006**, *128*, 3335–3345.
(33) Steinmetz, M. G.; Yu, C.; Li, L. *J. Am. Chem. Soc.* **1994**, *116*, 932–943.
(34) Sun, M. *Chem. Phys. Lett.* **2005**, *408*, 128–133.
(35) Valsson, O.; Filippi, C. *J. Chem. Theory Comput.* **2010**, *6*, 1275–1292.
(36) Muñoz-Losa, A.; Martín, M. E.; Galván, I. F.; Sánchez, M. L.; Aguilar, M. A. *J. Chem. Theory Comput.* **2011**, *7*, 4050–4059.
(37) Zgrablic, G.; Haacke, S.; Chergui, M. *J. Phys. Chem. B* **2009**, *113*, 4384–4393.
(38) Strambi, A.; Coto, P. B.; Frutos, L. M.; Ferré, N.; Olivucci, M. *J. Am. Chem. Soc.* **2008**, *130*, 3382–3388.
(39) Jang, G.; Kuksa, V.; Filipek, S.; Bartl, F.; Ritter, E.; Gelb, M. H.; Hofmann, K. P.; Palczewski, K. *J. Biol. Chem.* **2001**, *276*, 26148–26153.
(40) Hammond, G. *J. Am. Chem. Soc.* **1955**, *77*, 334–338.